

Article

Power-Law Compensator Design for Plants with Uncertainties: Experimental Verification

Stavroula Kapoulea ¹, Costas Psychalinos ^{1,*}, Ahmed S. Elwakil ^{2,3,4,*} and Mohammad Saleh Tavazoei ⁵

¹ Department of Physics, Electronics Laboratory, University of Patras, GR-26504 Rio Patras, Greece; skapoulea@upnet.gr

² Department of Electrical and Computer Engineering, University of Sharjah, Sharjah 27272, United Arab Emirates

³ Nanoelectronics Integrated Systems Center (NISC), Nile University, Giza 12588, Egypt

⁴ Department of Electrical and Computer Engineering, University of Calgary, Calgary, AB T2N 1N4, Canada

⁵ Electrical Engineering Department, Sharif University of Technology, Tehran 14588-89694, Iran; tavazoei@sharif.edu

* Correspondence: cpsychal@upatras.gr (C.P.); elwakil@ieee.org (A.S.E.)

Abstract: A power-law compensator scheme for achieving robust frequency compensation in control systems including plants with an uncertain pole, is introduced in this work. This is achieved through an appropriate selection of the compensator parameters, which guarantee that the Nyquist diagram of the open-loop system compensator-plant crosses a fixed point independent of the plant pole variations. The implementation of the fractional-order compensator is performed through the utilization of a curve-fitting-based technique and the derived rational integer-order transfer function is realized on a Field-Programmable Analog Array device. The experimental results confirm that the phase margin is well preserved, even for $\pm 40\%$ variation in the pole location of the plant.

Keywords: fractional-order controllers; fractional-order compensators; phase margin; crossover frequency; field-programmable analog array



check for updates

Citation: Kapoulea, S.; Psychalinos, C.; Elwakil, A.S.; Tavazoei, M.S.

Power-Law Compensator Design for Plants with Uncertainties:

Experimental Verification. *Electronics*

2021, 10, 1305. [https://doi.org/](https://doi.org/10.3390/electronics10111305)

10.3390/electronics10111305

Academic Editor: Flavio Canavero

Received: 25 April 2021

Accepted: 26 May 2021

Published: 30 May 2021

Publisher's Note: MDPI stays neutral with regard to jurisdictional claims in published maps and institutional affiliations.



Copyright: © 2021 by the authors. Licensee MDPI, Basel, Switzerland. This article is an open access article distributed under the terms and conditions of the Creative Commons Attribution (CC BY) license (<https://creativecommons.org/licenses/by/4.0/>).

1. Introduction

Fractional-order controllers are useful building blocks for compensating the existence of uncertainty in the model of a plant, which occurs in real-world control systems, and thus, many efforts towards the implementation of such blocks have been made [1–3]. The main feature of this family of controllers, which enables them to deal with uncertainty in control system loops, is the inherent flexibility of their structures [4], originating from the use of fractional operators with tunable orders. Robust fractional-order controllers can be designed based on the use of either time-domain methods [5] or frequency-domain ones [6]. Compared to time-domain approaches, frequency-domain methods provide a more powerful framework for optimal tuning of the tunable orders of the fractional operators in the structures of fractional controllers. For example, such controllers have been designed with the aim of offering flatness in the open-loop phase response around the gain crossover frequency [7–15] and have also been introduced to ensure robustness against variations in the time constant of a plant. In [16] a fractional-order controller was designed so that the phase margin and gain crossover frequency could have specific desired values. In [17] a fractional-order controller was proposed for stable minimum-phase plants with large uncertainty in the location of one of their poles. Following this, the rules introduced in [17] have been modified in [18] to include plants with fractional-order transfer functions and uncertain poles. The controller obtained from the method of [18] is able to exactly satisfy the required frequency-domain objectives, where the uncertain parameters in the plant model can vary in an infinite range. A further extension was done in [19] for the case of single-order power-law plant transfer functions. Furthermore, a fixed-structure fractional-order controller has been designed in [20] to obtain the desired values for the

phase margins and adjust the crossover frequencies. The method of [20] has been improved in [21] so that the uniqueness of the crossover frequencies is guaranteed.

In the present work, the tuning rules of [18] are applied in the case of plants with dynamics described by double-order power-law transfer functions, leading to the need for power-law compensators. The derived compensator transfer function is approximated through the utilization of a curve-fitting technique, resulting in a rational integer-order transfer function. This transfer function is capable of fulfilling the robust compensation problem of control systems, including plants with an uncertain pole [18] and can be implemented using conventional filter design techniques. As a design application example, a control system used in machining is presented and the performance of the introduced compensator, and also of the whole system, are evaluated through experimental results using a quad-core Field-Programmable Analog Array (FPAA) platform.

The paper is organized as follows: the proposed compensator is presented in Section 2, where both its theoretical analysis and implementation aspects are discussed. A design example and experimental results are presented in Section 3, certifying the validity of the presented concept.

2. Power-Law Compensator for Robustness against Plant Uncertainty

2.1. Theory

Consider a compensator-plant system, where the transfer function of the compensator is

$$C(s) = (k + qs^\alpha)^p, \quad (1)$$

with $\alpha \in (-2, 2)$, and the transfer function of the plant is given by

$$G_b(s) = \left(\frac{1}{bs^\beta + 1} \right)^p, \quad (2)$$

including an unknown parameter (b), possibly with a wide range of variation. The aim is to design the compensator such that the following objectives are met:

1. In the nominal case (i.e., $b = b_0$), the Nyquist diagram of the open-loop transfer function $T(s) = C(s) \cdot G_b(s)$ meets the fixed point $M \cdot e^{j\phi}$, where $M \in (0, \infty)$ and $\phi \in [-\pi, \pi)$, at a desired frequency $\omega = \omega_{c0}$;
2. Despite the variations of b from its nominal value, the Nyquist diagram of the transfer function still crosses the fixed point $M \cdot e^{j\phi}$.

The above objectives are simultaneously satisfied by the compensator if designed such that the following conditions hold:

$$\alpha = \beta + \frac{2\phi}{p\pi} - 2n, \quad n : \text{integer} \quad (3)$$

$$q = M^{1/p} \cdot \frac{\left[b_0 \omega_{c0}^\beta \sin\left(\frac{\beta\pi}{2} + \frac{\phi}{p}\right) + \sin\left(\frac{\phi}{p}\right) \right]}{\omega_{c0}^\alpha \sin\left(\frac{\alpha\pi}{2}\right)} \quad (4)$$

and

$$k = M^{1/p} \cdot \frac{\sin\left(\frac{\beta\pi}{2}\right)}{\sin\left(\frac{\beta\pi}{2} + \frac{\phi}{p}\right)}. \quad (5)$$

This can be proved using (3)–(5) and Theorem I in [18], where it is deduced that $(C(j\omega_{c0}) \cdot G_b(j\omega_{c0})|_{b=b_0})^{1/p} = M^{1/p} \cdot e^{j\phi/p}$. Therefore, $C(j\omega_{c0}) \cdot G_b(j\omega_{c0})|_{b=b_0} = M \cdot e^{j\phi}$ meets the first objective. In this case, each b , ω_c is found, such that $(C(j\omega_c) \cdot G_b(j\omega_c))^{1/p} = M^{1/p} \cdot e^{j\phi/p}$, thus confirming that the second objective is also satisfied. An important remark is that, for $M = 1$, the variable ϕ is related to the phase margin (PM) of the system

according to the formula $PM = \pi + \phi$, while the characteristic frequency is equal to the crossover gain frequency, i.e., $\omega_{c0} = \omega_{cg}$.

2.2. Design Example

In order to demonstrate that this concept is robust in stabilizing the PM of a controlled system in plants with uncertainties, we consider the problem of estimating the heat flux during machining, described in detail in [22]. The dynamics of the plant are described by a transfer function of the form

$$G_b(s) = \frac{1}{(bs^{0.92} + 1)^{1.49}}. \quad (6)$$

with nominal value $b = b_0 = 3.448$. Using the expressions in (3)–(5), and considering that $\phi = -\pi/2$, $M = 1$ (i.e., $PM = 90^\circ$ and that the crossover gain frequency is $\omega_{cg} = 20$ rad/s, then the transfer function of the required compensator becomes

$$C(s) = \left(2.5132 + 1.2495s^{0.2589}\right)^{1.49}. \quad (7)$$

The achieved robustness at the presence of uncertainty in the pole of the plant is demonstrated by considering a $\pm 40\%$ variation in the nominal value of b . The corresponding open-loop transfer function Nyquist plots, plotted in Figure 1 show that the PM was 89.97° at -40% deviation and 89.98° at $+40\%$ deviation; both are very close to the theoretical value of 90° .

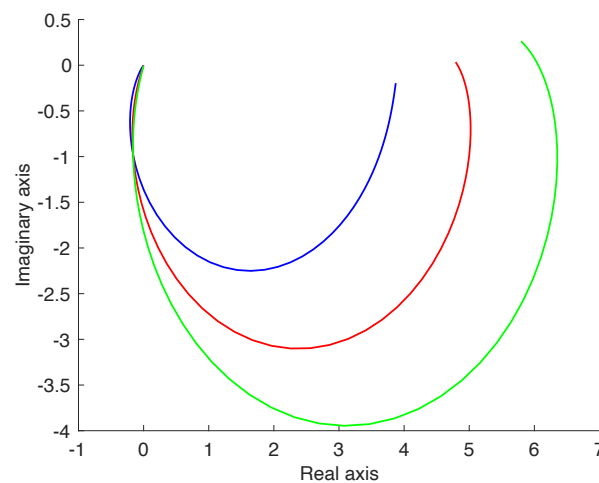


Figure 1. Nyquist plots of the controlled system (6) at the presence of plant uncertainties (blue: $b = 0.6b_0$, red: $b = b_0$, green: $b = 1.4b_0$).

The transfer function of the power-law compensator, given in (7), can be approximated using a curve-fitting technique based on the MATLAB built-in function *fitfrd*, which approximates the desired function within a pre-defined frequency range [23]. Another potential tool is the Padé approximation, which actually approximates the transfer function around a pre-defined center frequency. Here, the curve-fitting-based technique was employed since, in most cases, it provides improved accuracy over the Padé approximation tool [24,25]. The obtained rational integer-order transfer function which performs the approximation of its power-law counterpart within the frequency range $\omega = [10^0, 10^{+2}]$ rad/s, is given by

$$C(s) \simeq \frac{3.941 s^3 + 302.8 s^2 + 2608 s + 2041}{s^3 + 204.4 s^2 + 3836 s + 7708}. \quad (8)$$

A possible implementation of the function in (8) is that based on the standard Follow-the-Leader-Feedback (FLF) multi-feedback structure which is described by the transfer function

$$H_{FLF}(s) = \frac{G_3 s^3 + \frac{G_2}{\tau_1} s^2 + \frac{G_1}{\tau_1 \tau_2} s + \frac{G_0}{\tau_1 \tau_2 \tau_3}}{s^3 + \frac{1}{\tau_1} s^2 + \frac{1}{\tau_1 \tau_2} s + \frac{1}{\tau_1 \tau_2 \tau_3}}. \quad (9)$$

The variables τ_i , ($i = 1, 2, 3$) are time constants, while the variables G_j , ($j = 0, 1, 2, 3$) are gain factors and both are calculated through the equalization of the coefficients of the numerator and denominator in the polynomials in (8) and (9). The resulting values are provided in Table 1. It should be mentioned that (8) can also be implemented by other well-known structures, such as the Inverse-Follow-the Leader (IFLF) topology or the parallel filters topology. The IFLF topology is preferable in cases where differential signals are used while parallel filters are advantageous in the case of current-mode signals.

Table 1. Values of time constants and gain factors of the FLF structure for realizing the transfer function in (8).

Time Constants			Scaling Factors			
τ_1	τ_2	τ_3	G_0	G_1	G_2	G_3
4.9 ms	53.3 ms	497.7 ms	13.235	33.99	74.085	197.05

3. Experimental Verification

Field-Programmable Analog Arrays (FPAAs) are analog signal processors based on configurable analog blocks (CABs) that offer design programmability and versatility [26,27]. The functionality of the proposed compensator is evaluated through an experimental FPAA-based process, using the Anadigm AN231K04 FPAA [28]. The experimental setup is shown in Figure 2, where an extra interface stage, implemented on the breadboard using discrete AD844 operational amplifiers, is also used for the single-to-differential conversion of the input signal and the opposite conversion of the output signal of the FPAA. The power supply voltage is set as ± 15 V, while the chip clock is set as 1 kHz.

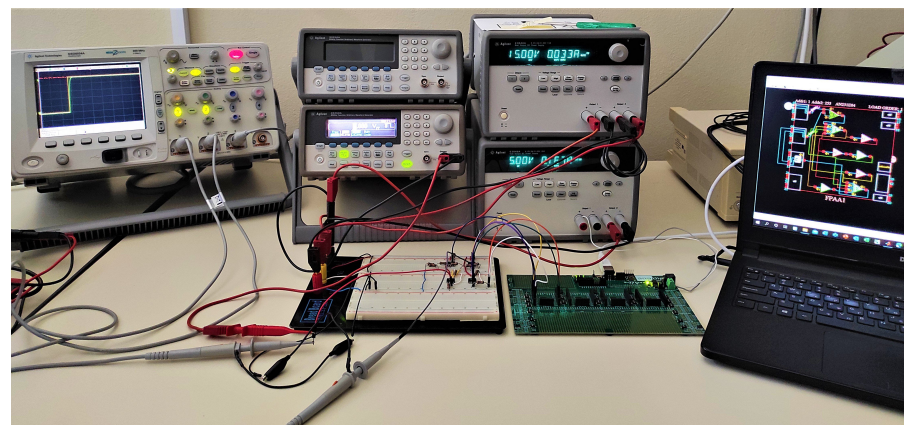


Figure 2. Experimental setup for evaluating the performance of the proposed power-law compensator.

3.1. Compensator-Plant System

The transfer function in (9) with the values of Table 1 was realized on the FPAA, as shown in the Anadigm design of Figure 3. Note that all gain factors were scaled by a factor equal to 0.02 to achieve reasonable results that avoid saturating the internal FPAA op-amps. This means that the realized function is $0.02 \times H_{FLF}(s)$. The integration stages of the FLF structure are implemented using *Integrator* CABs, while for the time constants of higher values, gain stages are also required. The feedback loop at the input point and the summation at the output point of the structure are realized through the two *Sum/Diff* CABs of the FPAA configuration.

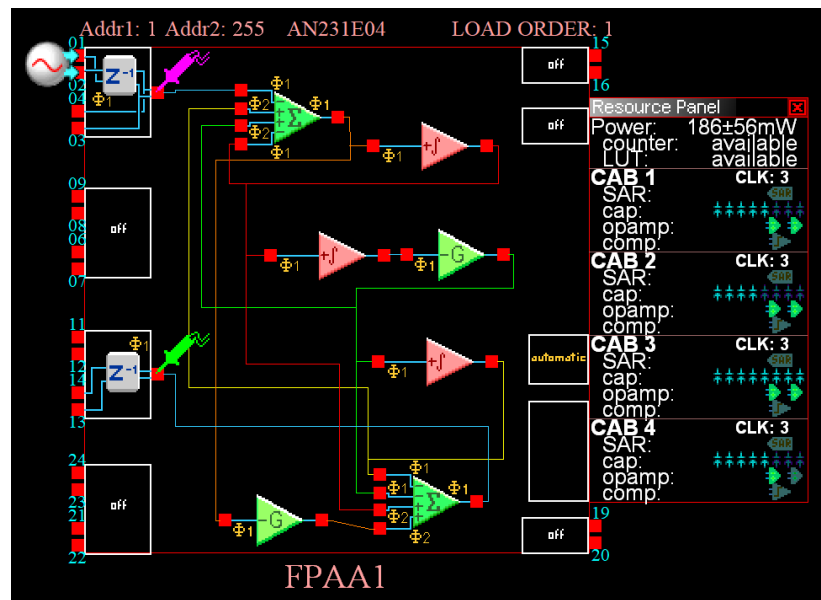
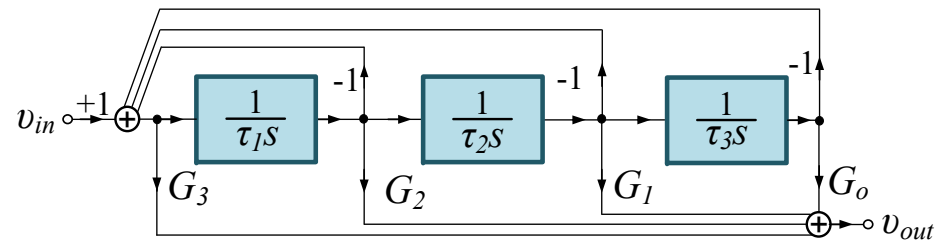


Figure 3. FLF structure and its realization on the FPA1.

The efficient operation of the realized compensator is evaluated through the obtained gain and phase frequency responses, depicted in Figure 4a, which are presented along with those predicted by the ideal compensator function in (7) and the approximated one in (8). The agreement between the experimental results and the corresponding approximated and ideal ones is evident and is further verified through the error plots of Figure 4b. The time-domain operation of the compensator is evaluated through the input and output waveforms at the crossover gain frequency $\omega_{cg} = 20 \text{ rad/s}$ with the obtained oscilloscope screenshot provided in Figure 4c. The measured gain and phase are 1.58 dB and 33° , with the corresponding theoretically predicted values being 1.56 dB and 33° , respectively.

Using the same configuration of Figure 3, the open-loop behavior of the system, i.e., the transfer function $C(s) \cdot G_b(s)$, can be evaluated. This is done after approximating the open-loop transfer function using the curve-fitting method in the form

$$C(s) \cdot G_b(s) \simeq \frac{-0.003221 s^3 + 19.78 s^2 + 257.4 s + 265.9}{s^3 + 12.97 s^2 + 17.48 s + 4.912} \quad (10)$$

with the corresponding FLF structure parameters summarized in Table 2.

Table 2. Values of time constants and gain factors of the FLF structure for realizing the transfer function in (10).

Time Constants			Scaling Factors			
τ_1	τ_2	τ_3	G_0	G_1	G_2	G_3
77.1 ms	742.1 ms	3.558 s	54.14	14.73	1.525	-0.0032

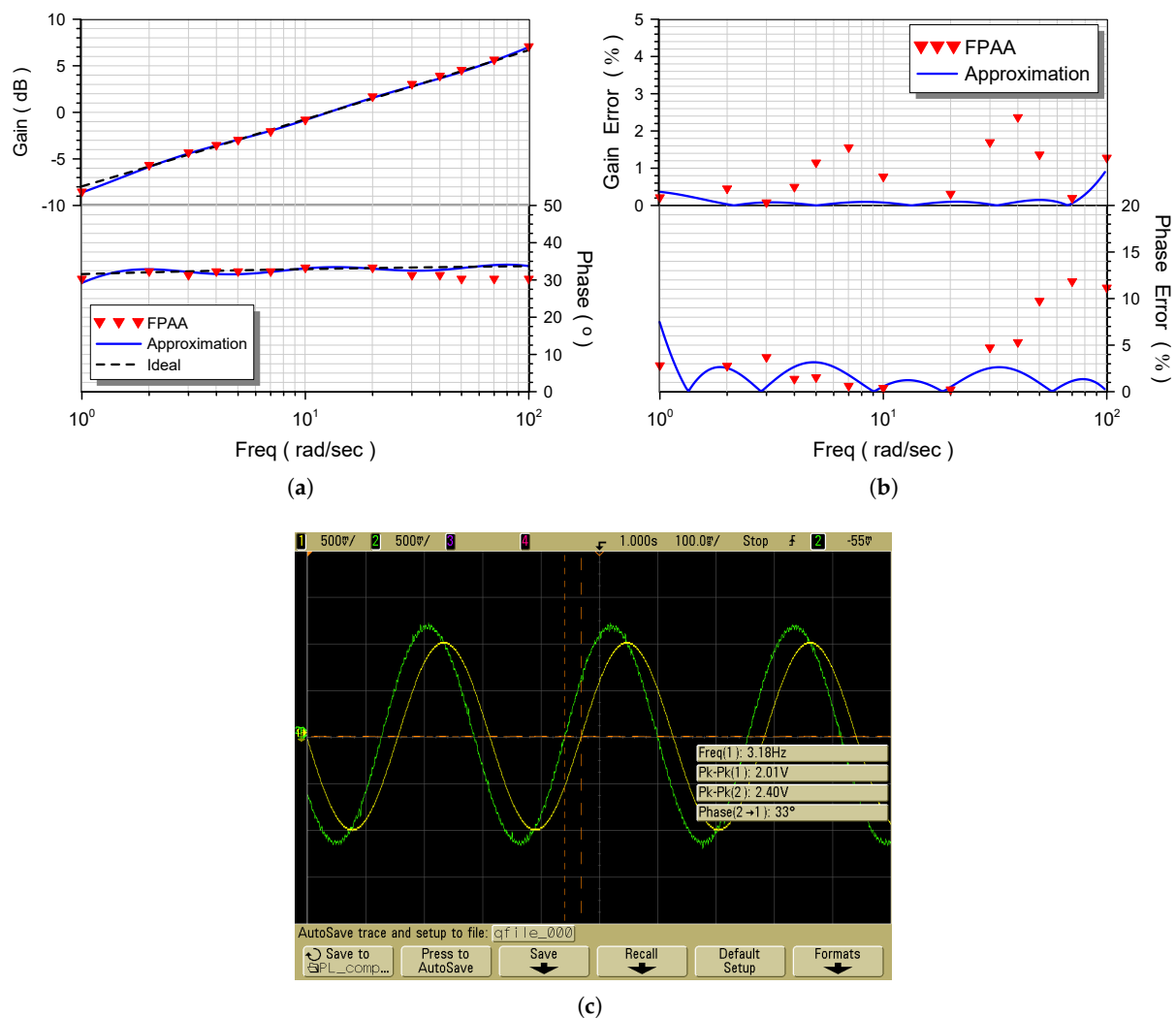


Figure 4. Experimental results of the realized power-law compensator (a) gain/phase responses and (b) their relative errors, and (c) input/output voltage waveforms at $\omega_{cg} = 20$ rad/s.

The open-loop frequency experimental behavior of the system is presented by the gain and phase plots in Figure 5a. The measured crossover gain frequency is 20 rad/s and the associated phase margin is 91° , close to the corresponding specification of 90° , while the corresponding relative errors are given by the plots of Figure 5b. The correct operation of the open-loop system is also verified by the time-domain plots in Figure 5c, where the oscilloscope screenshot (which presents the input and output waveforms at the characteristic frequency $\omega_{cg} = 20$ rad/s) are demonstrated.

The closed-loop compensator-plant system is implemented using an extra *Sum/Diff* CAB, in order to realize the feedback loop. The behavior of the system is evaluated through the step response (shown in the oscilloscope screenshot of Figure 6) with its efficiency being verified by the obtained results in the measurement of characteristic parameters. In particular, the measured values of the rise time, settling time and overshoot are 98 ms, 278 ms, and 0.1%, while the theoretically predicted values are 106.9 ms, 285.5 ms, and 0.1339%, respectively.

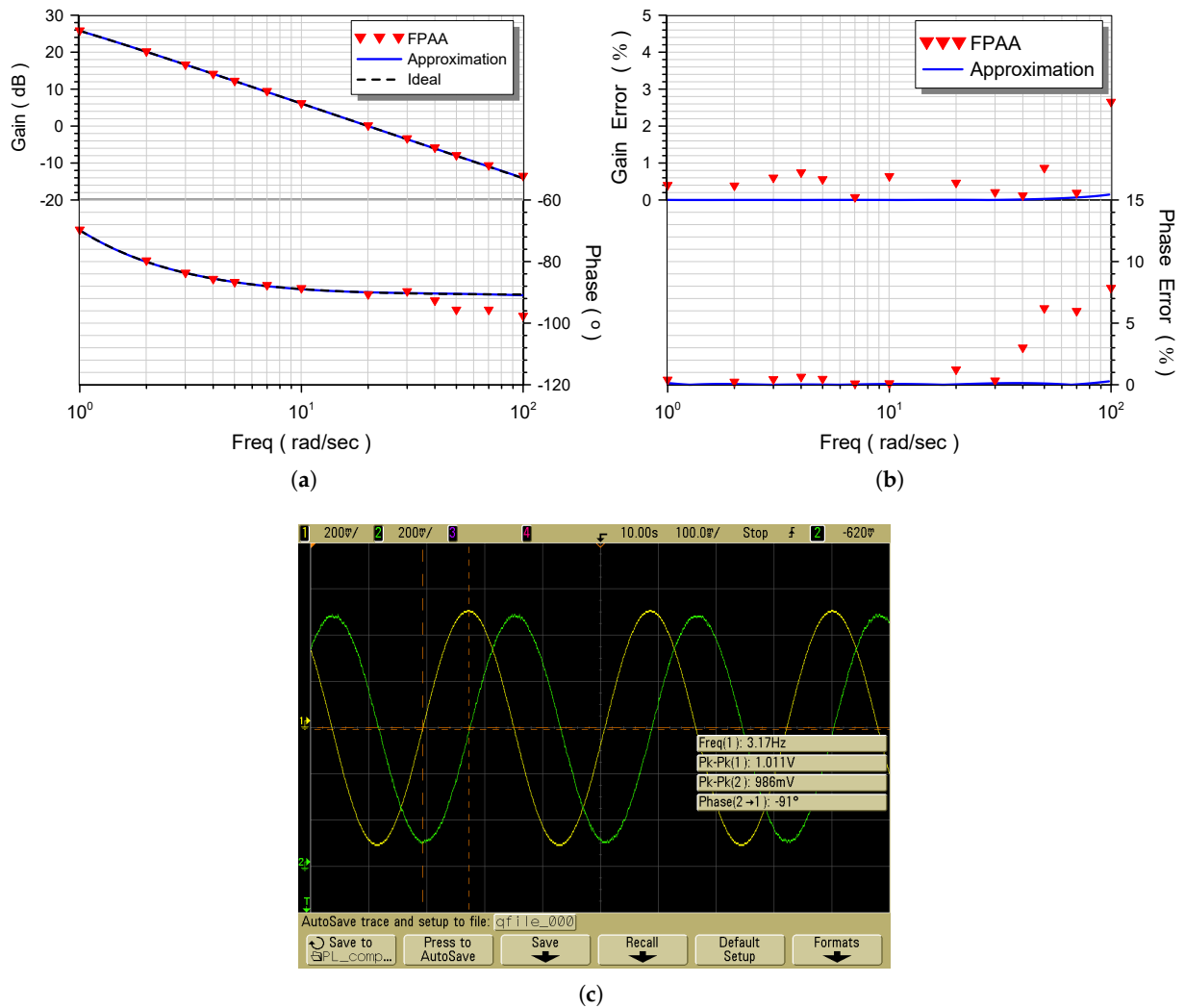


Figure 5. Experimental results of the open-loop system $C(s) \cdot G_b(s)$ (a) gain/phase frequency responses and (b) their relative errors, and (c) input/output voltage waveforms at the gain cross-over frequency $\omega_{gc} = 20$ rad/s.

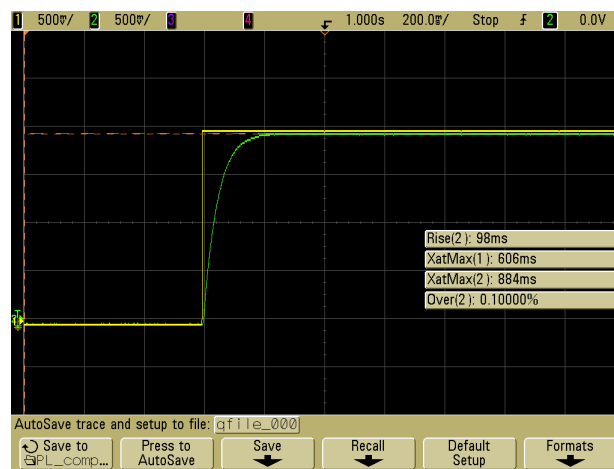


Figure 6. Experimental step response the closed-loop system at the nominal value of the pole of the plant.

3.2. Effect of the Plant Uncertainties

The effect of the uncertainty in the pole of the transfer function of the plant is experimentally studied, assuming that the variable b_0 is changed by $\pm 40\%$ of its nominal value. The behavior of the open-loop system towards these variations is evaluated through the input and output waveforms at the gain crossover frequency of 20 rad/s (see Figure 7a,b), where it is confirmed that the phase margin remains unaffected with values very close to the theoretically predicted value of 90° . The corresponding closed-loop system results, which are given by the oscilloscope screenshots of the step responses in Figure 7c,d, also verify, in this case, that the plant uncertainties do not affect the robustness of the fixed point. More specifically, the rise time is measured as (94, 100) ms and the settling time is measured as (288, 326) ms, respectively at -40% and $+40\%$ of the nominal pole value, with the ideal rise time being 98 ms and settling time being 278 ms.

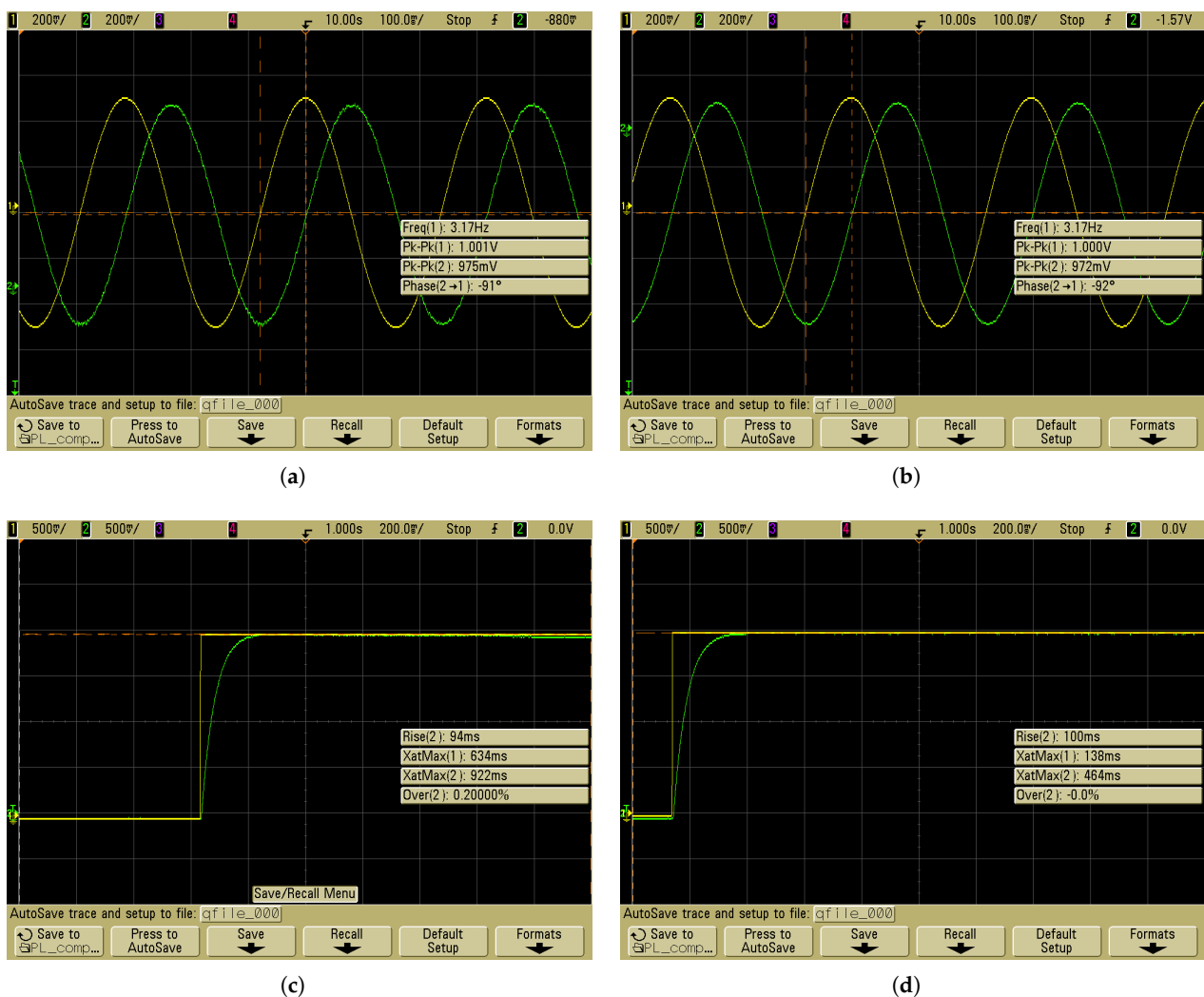


Figure 7. Input and output waveforms of the open-loop system at the characteristic frequency $\omega_{cg} = 20$ rad/s in the presence of the plant's pole uncertainty and corresponding step responses (a,c) $b = 0.6 \cdot b_0$ and (b,d) $b = 1.4 \cdot b_0$.

4. Conclusions

Robust compensation of the frequency response characteristics of plants described by power-law dynamics can be achieved through the utilization of compensators, also described by a power-law transfer function. This is achieved through the establishment of suitable tuning rules, which perform appropriate shaping of the open-loop Nyquist plot in such a way that it always crosses a desired point. This is very important from a

practical perspective because the invariant phase and gain margins can be considered as special cases of the aforementioned feature, making the derived control system robust in fractional-order plants with an uncertain pole. A selected design example is experimentally verified using an FPAA-based implementation, verifying the theoretical results.

Author Contributions: Conceptualization, C.P. and A.S.E.; methodology, C.P.; software, S.K.; validation, S.K. and C.P.; formal analysis, M.S.T.; investigation, S.K. and C.P.; writing—original draft preparation, S.K. and C.P.; writing—review and editing, C.P., A.S.E. and M.S.T.; project administration, C.P. and A.S.E. All authors have read and agreed to the published version of the manuscript.

Funding: This research received no external funding.

Data Availability Statement: No new data were created or analyzed in this study. Data sharing is not applicable to this article.

Acknowledgments: This research is co-financed by Greece and the European Union (European Social Fund-ESF) through the Operational Programme “Human Resources Development, Education and Lifelong Learning” in the context of the project “Strengthening Human Resources Research Potential via Doctorate Research-2nd Cycle” (MIS-5000432), implemented by the State Scholarships Foundation (IKY).

Conflicts of Interest: The authors declare no conflict of interest.

Abbreviations

The following abbreviations are used in this manuscript:

CAB	Configurable analog block
FLF	Follow the leader feedback
FPAA	Field programmable analog array
IFLF	Inverse follow the leader feedback
FBD	Functional block diagram
PM	Phase margin

References

1. Caponetto, R.; Dongola, G.; Maione, G.; Pisano, A. Integrated technology fractional order proportional-integral-derivative design. *J. Vib. Control* **2014**, *20*, 1066–1075. [[CrossRef](#)]
2. Muñoz-Montero, C.; García-Jiménez, L.V.; Sánchez-Gaspariano, L.A.; Sánchez-López, C.; González-Díaz, V.R.; Tlelo-Cuautle, E. New alternatives for analog implementation of fractional-order integrators, differentiators and PID controllers based on integer-order integrators. *Nonlinear Dyn.* **2017**, *90*, 241–256. [[CrossRef](#)]
3. Dimeas, I.; Petras, I.; Psychalinos, C. New analog implementation technique for fractional-order controller: A DC motor control. *AEU Int. J. Electron. Commun.* **2017**, *78*, 192–200. [[CrossRef](#)]
4. Tavakoli-Kakhki, M.; Haeri, M.; Tavazoei, M.S. Simple fractional order model structures and their applications in control system design. *Eur. J. Control* **2010**, *16*, 680–694. [[CrossRef](#)]
5. Tavazoei, M.S. Time response analysis of fractional-order control systems: A survey on recent results. *Fract. Calc. Appl. Anal.* **2014**, *17*, 440–461. [[CrossRef](#)]
6. Padula, F.; Visioli, A. *Advances in Robust Fractional Control*; Springer: Berlin/Heidelberg, Germany, 2015.
7. Luo, Y.; Chen, Y. Fractional-order [Proportional Derivative] controller for robust motion control: Tuning procedure and validation. In Proceedings of the 2009 American Control Conference, St. Louis, MO, USA, 10–12 June 2009; pp. 1412–1417.
8. Luo, Y.; Chen, Y.Q.; Wang, C.Y.; Pi, Y.G. Tuning fractional order proportional integral controllers for fractional order systems. *J. Process. Control* **2010**, *20*, 823–831. [[CrossRef](#)]
9. Luo, Y.; Chen, Y. Stabilizing and robust fractional order PI controller synthesis for first order plus time delay systems. *Automatica* **2012**, *48*, 2159–2167. [[CrossRef](#)]
10. Luo, Y.; Zhang, T.; Lee, B.; Kang, C.; Chen, Y. Fractional-order proportional derivative controller synthesis and implementation for hard-disk-drive servo system. *IEEE Trans. Control Syst. Technol.* **2013**, *22*, 281–289. [[CrossRef](#)]
11. Basiri, M.H.; Tavazoei, M.S. On robust control of fractional order plants: Invariant phase margin. *J. Comput. Nonlinear Dyn.* **2015**, *10*, 054504. [[CrossRef](#)]
12. Dastjerdi, A.A.; Saikumar, N.; HosseinNia, S.H. Tuning guidelines for fractional order PID controllers: Rules of thumb. *Mechatronics* **2018**, *56*, 26–36. [[CrossRef](#)]
13. Dastjerdi, A.A.; Vinagre, B.M.; Chen, Y.; HosseinNia, S.H. Linear fractional order controllers; A survey in the frequency domain. *Annu. Rev. Control* **2019**, *47*, 51–70. [[CrossRef](#)]

14. Li, X.; Gao, L. Robust Fractional-order PID Tuning Method for a Plant with an Uncertain Parameter. *Int. J. Control Autom. Syst.* **2021**, *19*, 1302–1310. [[CrossRef](#)]
15. Tepljakov, A.; Alagoz, B.B.; Yeroglu, C.; Gonzalez, E.A.; Hosseinnia, S.H.; Petlenkov, E.; Ates, A.; Cech, M. Towards Industrialization of FOPID Controllers: A Survey on Milestones of Fractional-Order Control and Pathways for Future Developments. *IEEE Access* **2021**, *9*, 21016–21042. [[CrossRef](#)]
16. Jin, Y.; Chen, Y.Q.; Xue, D. Time-constant robust analysis of a fractional order [proportional derivative] controller. *IET Control Theory Appl.* **2011**, *5*, 164–172. [[CrossRef](#)]
17. Feliu-Batlle, V.; Castillo-García, F.J. On the robust control of stable minimum phase plants with large uncertainty in a time constant. A fractional-order control approach. *Automatica* **2014**, *50*, 218–224. [[CrossRef](#)]
18. Sayyaf, N.; Tavazoei, M.S. Robust fractional-order compensation in the presence of uncertainty in a pole/zero of the plant. *IEEE Trans. Control Syst. Technol.* **2018**, *26*, 797–812. [[CrossRef](#)]
19. Basiri, M.H.; Tavazoei, M.S. Robust Control of a Class of Fractional Order Plants in the Presence of Pole Uncertainty. In Proceedings of the Electrical Engineering (ICEE), Iranian Conference on, Mashhad, Iran, 8–10 May 2018; pp. 881–886.
20. Sayyaf, N.; Tavazoei, M.S. Desirably adjusting gain margin, phase margin, and corresponding crossover frequencies based on frequency data. *IEEE Trans. Ind. Inform.* **2017**, *13*, 2311–2321. [[CrossRef](#)]
21. Sayyaf, N.; Tavazoei, M.S. Frequency data-based procedure to adjust gain and phase margins and guarantee the uniqueness of crossover frequencies. *IEEE Trans. Ind. Electron.* **2020**, *67*, 2176–2185. [[CrossRef](#)]
22. Sommacal, L.; Melchior, P.; Oustaloup, A. Havriliak-Negami function for thermal system identification. In Proceedings of the 2008 American Control Conference, Seattle, WA, USA, 11–13 June 2008; pp. 1316–1321.
23. Kapoulea, S.; Psychalinos, C.; Elwakil, A.S. Power law filters: A new class of fractional-order filters without a fractional-order Laplacian operator. *AEU Int. J. Electron. Commun.* **2021**, *129*, 153537. [[CrossRef](#)]
24. Kapoulea, S.; Tsirimokou, G.; Psychalinos, C.; Elwakil, A.S. Employment of the Padé approximation for implementing fractional-order lead/lag compensators. *AEU Int. J. Electron. Commun.* **2020**, *120*, 153203. [[CrossRef](#)]
25. Kapoulea, S.; Psychalinos, C.; Elwakil, A.S. Double Exponent Fractional-Order Filters: Approximation Methods and Realization. *Circuits Syst. Signal Process.* **2021**, *40*, 993–1004. [[CrossRef](#)]
26. Muñoz-Montero, C.; Sánchez-Gaspariano, L.A.; Sánchez-López, C.; González-Díaz, V.R.; Tlelo-Cuautle, E. On the electronic realizations of fractional-order phase-lead-lag compensators with OpAmps and FPAs. In *Fractional Order Control and Synchronization of Chaotic Systems*; Springer: Berlin/Heidelberg, Germany, 2017; pp. 131–164.
27. Tlelo-Cuautle, E.; Pano-Azucena, A.D.; Guillén-Fernández, O.; Silva-Juárez, A. *Analog/Digital Implementation of Fractional Order Chaotic Circuits and Applications*; Springer: Berlin/Heidelberg, Germany, 2020.
28. Anadigm. *AN231E04 dpASP: The AN231E04 dpASP Dynamically Reconfigurable Analog Signal Processor*; Anadigm: Mesa, AZ, USA, 2021.